# Dynamic Modeling of Nuclear Fusion As a New Tool to Identify Subgroups in Multiple Sclerosis Magnetic Resonance Imaging Data

Heiko Neeb

***Abstract*—A key problem in the MR-based diagnosis of multiple sclerosis (MS) is the observed mismatch between clinical and imaging findings. One of the most promising approaches to overcome those problems is based on quantitative magnetic resonance imaging (qMRI), where physiological parameters such as proton diffusion or absolute myelin water content are directly measured. Consequently, combining the quantitative image measures with automated analysis schemes might result in the definition of new biomarkers which better correlate with the clinical disability. The current work describes a new approach for the unsupervised grouping of individual patients, where each subject is considered as a point in an $N$-dimensional feature space. The points are dynamically modeled as nucleons (protons or neutrons) which experience an attractive force at short distances while repelling each other at longer distances. Therefore, clusters of nearby points form larger objects ('nuclei') while outliers are pushed further away. In the current paper, initial results from a group of 43 MS subjects are presented along with a description of the underlying modeling algorithm and its validation on artificial test data. In the patient study, have observed that subjects with mild disease without neurological symptoms formed a homogeneous cluster. In contrast, patients with significant disease burden and heterogenous treatment histories were classified as outliers. The results demonstrate the potential of the new approach for an unsupervised classification of MS patients into clinically relevant subgroups using quantitative MRI data.**

***Index Terms*—Quantitative magnetic resonance imaging, dynamic modeling, cluster analysis, outlier removal, multiple sclerosis.**

## I. Introduction

MULTIPLE sclerosis is the most common neurodegenerative disorder in the first decades of live. The underlying pathogenesis is largely governed by demylination, axonal/neuronal damage and inflammation [1]. Magnetic resonance imaging is one of the cornerstones for the ultimate diagnosis of the disease, in addition to the neurological appearance of patients [2]. However, it is only of very limited use for an objective disease follow-up and for therapy monitoring [3], [4]. Therefore, new MR metrics have been extensively investigated in the literature in order to overcome the mismatch between clinical and imaging findings.

In the recent past, quantitative magnetic resonance imaging (qMRI) has emerged as a promising tool for the more objective characterisation and follow-up of multiple sclerosis. Several authors have quantified changes in tissue relaxation times, diffusion, proton density or magnetisation transfer ratio in various stages of the disease, during therapy or between different clinical subgroups [5]–[12]. Furthermore, the amount of water bound between the myelin bilayers is one of the parameters which is supposed to be much more specific to the underlying MS pathology. Originally initiated by the seminal work of MacKay et al. [13], myelin water content mapping has gained a lot of attention in the recent past, where many new approaches for its quantification have been published [14]–[21]. However, most of the new methods either suffer from prolonged measurement times or limited spatial coverage. Moreover, only myelin water content is quantified while other parameters, which reflect different aspects of the disease, often cannot be reconstructed from the same image data.

In order to overcome those problems, a new approach for the simultaneous quantification of tissue $T_1$ and $T_2^*$ relaxation times as well as total and myelin bound water content has recently been published by our group [22]–[24]. The method is fast and allows for a high resolution full brain mapping in approx. 10 minutes. The simultaneous acquisition of multiple parameters naturally leads to the application of multivariate analysis strategies. Such approaches are based on the combination of different parameters such as $T_1$ and $T_2^*$ to form a high dimensional vector, defined in the so called *feature space*. These methods offer the possibility to include higher dimensional correlations between parameters, thereby increasing their classfication performance. It can thus be speculated that an improved prediction of disease grade or therapy response might be feasible based on a proper multidimensional combination of $T_1$,$T_2^*$ as well as total and myelin water content.

However, one has to be carefull with the naive application of multivariate tools as MR parameters are biophysically correlated. This results in a none-spherical distribution of points in feature space which severly restricts the use of standard unsupervised methods such as cluster analysis. The latter refers to a class of different powerfull tools which are sucessfully employed for the identification of groups or "clusters" of similar points in many applications (see e.g. [25]). Most of the standard approaches such as hierarchical or $k$-means clustering require the definition of a distance between points in the $N$-dimensional feature space. However, the often employed Euclidean distance favours the generation of spherical clusters due to the isotropic nature of this measure [25]. Therefore, the above cited methods are not appropriate for the identification of clusters in correlated datasets where none-spherical clusters are typically observed.

Moreover, cluster analysis is designed to find dense regions in feature space. The corresponding regions are then

Manuscript received July 4, 2012; revised August 09, 2012.

H. Neeb is with the Department of Mathematics and Technology, University of Applied Sciences Koblenz, 53424 Remagen, Germany, e-mail: neeb@rheinahrcampus.de (see http://www.rheinahrcampus.de/ImagingPhysics.html).

interpreted as homogeneous groups where all member behave similar. However, the identification of a "group" of patients, responding heterogenously to a given therapy, could be of relevance for a proper classification of the success or failure of a clinical intervention. From the pattern classification perspective, such points have to be treated as outliers which cannot be assigned to a common cluster. However, such an outlier subgroup cannot be detected using standard methods which are designed to find dense clusters only.

The current work presents a new approach for the identification of clusters which can be arbitrarily distributed in $N$-dimensional feature space. Moreover, the method inherently allows for the simultaneous detection of outliers. It is based on a simplified dynamic modeling of nuclear fusion, where larger nuclei are successively beeing build up from individual nucleons. Each datapoint is therefore modeled as a proton. The protons are initially placed in an $N$-dimensional space at a location given by their corresponding feature vectors. The formation of clusters is then governd by the strong interaction at short distances, which binds protons by exchanging charged or neutral virtual pions [26]. On the other hand, outliers are more or less randomly distributed in space. Therefore, they experience only the repulsive electromagnetic force resulting from the exchange of virtual photons [27]. This results in an attraction of nearby points which dynamically form high density clusters whereas all outliers are pushed away from the corresponding dense regions as $t \to \infty$.

The whole approach, named *Nuclear Potential Clustering (NPC)*, was tested on synthetic datasets to demonstrate the general performance of the algorithm. Furthermore, 43 MS patients with different disease grade and heterogeneous treatment histories where investigated using features dervied from quantitative $T_1$, $T_2^*$, total and myelin water content maps.

## II. Methods

### A. MR Data acquisiton and processing

43 MS patients with an age of $40.5 \pm 11.1$ years (18 male and 25 female) were scanned on a 3T Trio MR scanner (Siemens, Erlangen/Germany). The disease grade was evaluated by the EDSS score [2] and ranged between 0 and 6.5 in the cohort studied here. For each patient, quantitative maps of $T_1$, $T_2^*$ and total water content were reconstructed from two multiecho gradient echo sequences and 3 EPI scans [22]. Furthermore, the absolute myelin water content was obtained from the same data as described in [24]. In total, 50 transverse slices with a thickness of $2mm$ and an in-plane resolution of $1 \times 1mm^2$ were reconstructed. The total measurement time was $\approx 10min$.

All maps were warped to the common MNI152 space using FSL (www.fmrib.ox.ac.uk/fsl, [28]) and subsequently segmented into white matter (WM), grey matter (GM) and cerebrospinal fluid (CSF) using $T_1$ maps [29]. For each slice, each segment (WM and GM) and each map, features such as the average of each parameter, higher order moments or the spatial correlation distance were calculated [29]. In total, 450 features $(x_1, x_2, ...x_{450})$ were determined for each subject. The corresponding feature vector $\vec{x} = (x_1, x_2, ...x_{450})$ defines the inital position of the corresponding point (nucleon) in a 450-dimensional space.

### B. Nuclear Potential Clustering

*1) Potential function:* Each nucleon[1] with initial coordinates given by $\vec{x} = \vec{x}(t=0) = (x_1, x_2, ...x_n)$ experiences an effective potential from all other nucleons, given by the superposition of a short range strong interaction and a long range Coulomb term. The effective interaction within a nucleus is defined by a Woods-Saxon ansatz [30]

$$\phi^s(r) = \frac{-V_0}{1 + e^{\frac{r-R}{a}}}, \tag{1}$$

whereas the repulsive term outside the nuclei is given by the well known expression for the Coulomb potential, $\phi^c(r) = r^{-1}$. Here, the electic charge was normalised to $4\pi\epsilon_0$. In Equation (1), $r$ defines the distances (e.g. Euclidean) between two points in feature space, $R$ is the typical radius where the strong interaction is effective and $a$ defines the slope of the potential at the border where it starts to increase from $-V_0$ to 0 [30]. The strength of the interaction is given by $V_0 > 0$. As (1) defines the resulting potential within a distance R from the origin, the Coulomb term is effective only for distances larger than the typical radius of a nucleus, $R$.

In order to assign numbers to the free parameters $V_0$, $R$ and $a$, the data were first normalised by replacing $x_i \to (x_i - \bar{x_i})/\sigma_{x_i}$. Here, $\bar{x_i}$ ($\sigma_{x_i}$) is the average (standard deviation) of the $i^{th}$ feature, calculated from all points to be clustered. The following values were empirically chosen based on the observed perfomance of the algorithm on different test datasets where number, shape and density of clusters as well as the dimension of feature space were varied: $V_0 = 3500$, $R = 10\%$ quantile of the initial $(t = 0)$ distance distribution between all points and $a = R/50$. The radius $R$ is thus adpoted to each dataset based on the measured distribution of mutual distances between all points. Using these parameters, a similar performances of the algorithm was observed for all datasets, as long as the data were properly normalised.

*2) Dynamic modeling:* Based on the initial distribution of features, $\vec{x_i}(t=0); i = 1...n$, the total potential $\phi$ at the location of each of the $n$ points is calculated. As nucleons are modeled as classical particles moving in a superposition of strong and electromagnetic force fields, they obey the Newtonian equation of motion,

$$\frac{d^2}{dt^2}\vec{x_i} + \tau\frac{d}{dt}\vec{x_i} = -\vec{\nabla}\phi(\vec{x_i}). \tag{2}$$

It is important to notice that the force, $\vec{F_i} = -\vec{\nabla}\phi(\vec{x_i})$, is a function of time because the positions of each point in feature space, $\vec{x_i}(t)$, change with time according to Eq. (2). The damping term $\tau d\vec{x_i}/dt$ was introduced to model the capture of one nucleon in the field of another. If the kinetic energy of a nucleon is larger than the depth of the strong potential well (Eq. (1)), the nucleon will be scattered rather than beeing bound in the case of $\tau = 0$. However, the damping term avoids this effect and results in a quicker transition to an equalibrium state, making the algorithm significantly faster. In all our examples, the damping constant was set to $\tau = 200[a.u.]$, although the algorithm was largely immue agains variations of $\tau$.

[1]The words "point" and "nucleon" as well as "cluster" and "nucleous" are used synonymously throughout the text.

ISBN: 978-988-19251-6-9
ISSN: 2078-0958 (Print); ISSN: 2078-0966 (Online)

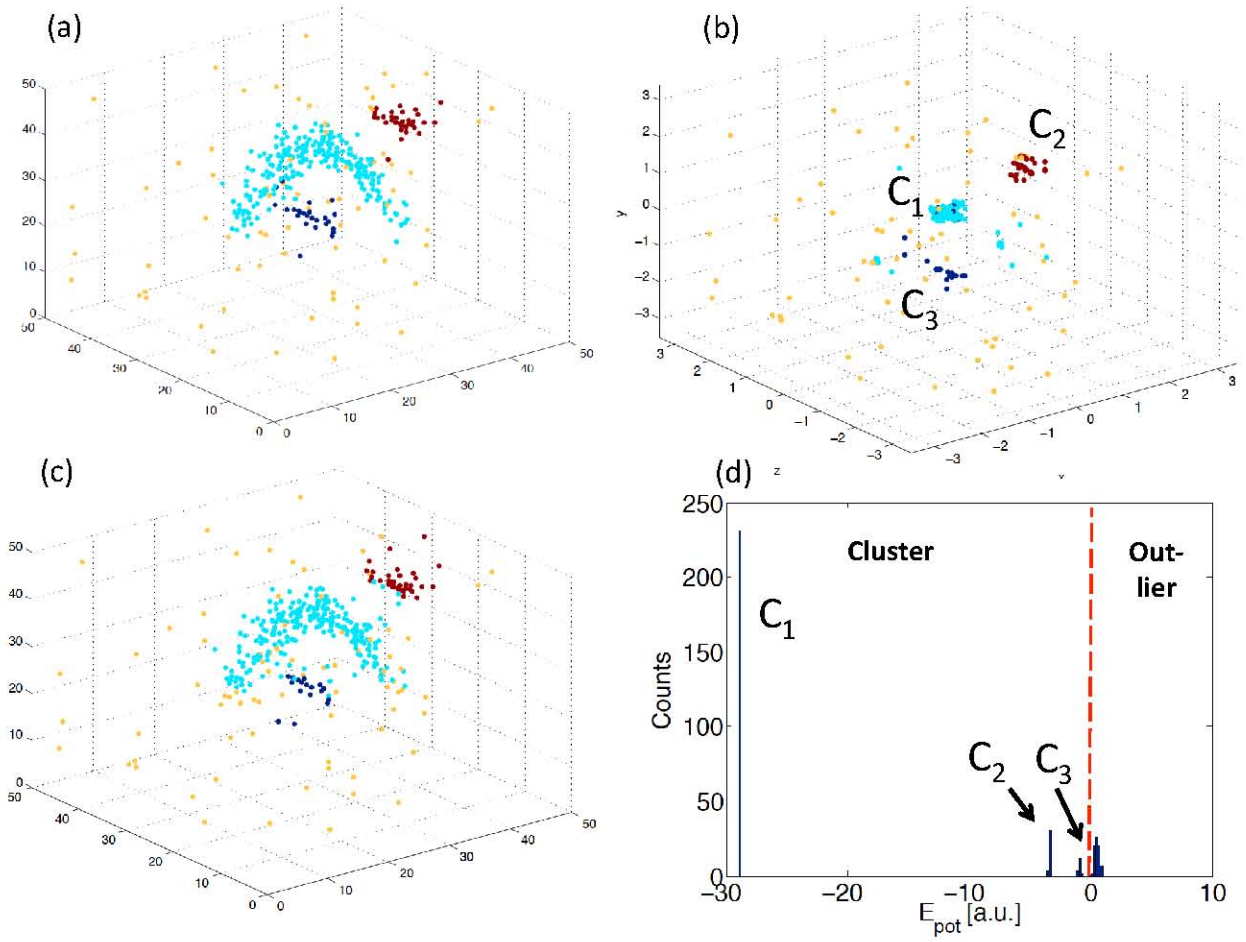


Fig. 1. Results from the application of *Nuclear Potential Clustering* on an artificial dataset, consisting of a horseshoe and two blops, overlaid by random noise. (a) Initial distribution of points in 3D feature space. The three clusters are shown in cyan, blue and brown, whereas the group of outliers is indicated by the yellow points. (b) Distribution of points in space at the end of the dynamic modeling. Three dense "spherical nuclei" were formed from nucleons which were initially spread out in space. (c) Automated classification of three clusters. (d) Histogram of the final potential energy of all points. Outliers are identified by $\bar{E}^{pot} > 0$ whereas the other three clusters, named $C_1$, $C_2$ and $C_3$, respectively, are identified by the corresponding peaks in the distribution.

Equation (2) was numerically integrated using a Runge-Cutta $4^{th}$ order solver. At each time step, the system temperature $T(t)$ was determined, defined as the average kinetic energy of all points. The time dependence of the temperature was subsequently used to define an objective stopping criterion for the algorithm. As points attract each other to form clusters, they gain velocity by decreasing their potential energy. In consequence, the average distance between points decreases along with $\phi$. Later, the kinetic energy will again decrease by increasing the distance between points. This interchange between both forms of energy continues until the systems reaches its equalibrium state of zero velocity for all particles, where larger nuclei have been formed. Therefore, $T(t)$ strongly resembles the curve of an anharmonic damped oscillation with different frequencies. The dynamic modeling automatically stops when the system temperature is less than $1\%$ of the value it takes at the corresponding maximum. Finally, the potential energy of each particle is determined which will be required for the definition of cluster memberships (see below).

*3) Repetition for different velocities:* The steps described in section II-B2 were repeated 5 times with different initial velocities for each particle. During the first run, the particles start at rest, i.e. $d\vec{x}_i/dt(t=0) = 0$. For the $i^{th}$ repetition $(i > 1)$, the initial velocities were randomly sampled from a zero mean Gaussian distribution where the standard deviation is given by the maximum kinetic energy of the particles during the $i-1^{st}$ step. Random initial velocities were chosen to ensure that nearby particles have a finite chance to overcome the Coulomb barrier and fuse with other particles, even if their distance is larger than the range of the strong potential. Furthermore, it supresses the spurious assignment of outlier points to clusters.

*4) Cluster identification:* Finally, the mean potential energy, $\bar{E}^{pot}$, of each point was determined by averaging the corresponing values from all five repetitions. Points belonging to larger clusters possess a negative potential energy as they experience the nuclear force field from other nucleons. In contrast, a positive potential energy is observed for outliers as they only see the long ranging positive part of the total potential. Furthermore, points located in the same cluster are easily identifiable as they have, on average, the same number of neighbours and therefore the same potential energy. Therefore, different clusters were identifying by searching for peaks in the distribution of $\bar{E}^{pot}$.

ISBN: 978-988-19251-6-9
ISSN: 2078-0958 (Print); ISSN: 2078-0966 (Online)

### C. Synthetic data

To validate the approach on correlated datasets, synthetic data consisting of three clusters with different shapes were created. Here, a "horseshoe and blop" configuration was chosen as shown in Fig. 1(a). The horseshoe consists of 228 points (63.4%) whereas the two blops contained 25 (6.9%) and 35 (9.8%) points, respectively. Moreover, 70 (19.5%) points were randomly placed in feature space to study the performance of the *Nuclear Potential Clustering* approach for outlier detection. In the current work, a three dimensional feature space was chosen in order to allow for a direct visualisation of the clusters formed. Corresponding tests of the algorithm on higher dimensional data yielded a similar performance as in the 3D case. Given the linearity of the equations of motion (Eq. 2), the isotropic nature of the Euclidean distance and the adaptive determination of the strong interaction range, one would indeed not expect a significant perfomances drop in higher dimensional data.

## III. Results

Fig. 1 shows the results obtained from the investigation of the artificial dataset. The initial horseshoe and blop configuration in 3D space is shown in Fig. 1(a). At the end of the dynamic modeling, all three clusters were shrunken to nearly spherical regions, filling a much smaller part of feature space (Fig. 1(b)). The final unsupervised assignment of points to clusters and outliers is shown in Fig. 1(c), where a high degree of similarity with the known configuration is observed. The identification of clusters was based on the average potential energy of each point as described above. Fig. 1(d) shows the corresponding distribution of $\bar{E}^{pot}$. All groups can easily be identified by four distinct peaks in the histogram.

Results from the automated clustering of MS patient data is shown in Fig. 2. The temperature initially shows a steep increase due to the strong attraction of nearby nucleons. At later times, an oszillating behaviour with different frequencies is observed, before the curve declines to zero due to the strong damping factor (see Fig. 2(a)). Our algorithm identified two distinct groups in the MS datasets (Fig. 2(b)). The first larger group consists of a dense homogeneous cluster. Furthermore, a smaller "outlier" group with $\bar{E}^{pot} \geq 0$ was discovered. In order to investigate the possible pathological and phenotypic correlates of this observation, the average EDSS score as well as the age and gender distribution of both groups were determined (see Table I and Fig. 2(c)). The outlier group is on average 8.3 years older and exhibits a higher disease grade as evaluated by the EDSS score. In contrast, the homogeneous cluster is dominated by patients with the lowest possible disease grade, EDSS=0 (Fig. 2(c)). This observation can be interpreted as a heterogeneous spreading of points in feature space as a result of either (1) disease progression and/or (2) increasing age. However, the results are very preliminary and need to be interpreted with care. The group size investigated is rather small and other phenotypes such as the disease subtype of were not controlled for. Nevertheless, the results clearly demonstrate the potential of our new approach to reveal underlying structures in high dimensional quantitative MRI datasets.

TABLE I
MS Data Clustering Results

| Cluster | $N$ | EDSS | Age [Years] | Gender |
|---|---|---|---|---|
| $E_{pot} \geq 0$ | 14 | $2.5 \pm 2.2$ | $46.1 \pm 12.4$ | 8 Male, 6 Female |
| $E_{pot} < 0$ | 29 | $0.9 \pm 1.6$ | $37.8 \pm 9.7$ | 9 Male, 20 Female |

## IV. Discussion and Conclusion

In the current work, a new method for the unsupervised grouping of points in multidimensional feature space was presented. The method is based on a simplified classical model for the formation of larger nuclei from the fusion of single nucleons or smaller nuclei. Its performance has been tested in correlated artificial datasets and in multidimensional quantitative MR image features defined for a group of 43 multiple sclerosis patients.

### A. Performance of the algorithm

As demonstated in the results section, the algorithm presented in the current work offers the possibility to automatically determine the number of clusters. This is achieved by stopping the iterative approach at the point of lowest average kinetic energy. Here, the system has reached its equalibrium state where larger nuclei have been formed. As can be seen from Fig. 1, the corresponding clusters are nearly spherical. This is not unexpected as the Euclidean distance between nuclei was employed in the corresponding potential function. In contrast, clustering approaches such as $k$-means result in the formation of spherical clusters when using the Euclidean distance measure as no dynamic rearrangement of points in space is performed [25]. This limits their applicability to none correlated dataset where isotropic groups are expected.

In our model, the total depth of the potential in the fused nuclei decreases with increasing size. Furthermore, it is approximately constant for all constitutents as the Woods-Saxon function is almost flat for distances $r < R$ (Eq. 1). The latter point is important as it provides the basis for the indentification of points belonging to the same cluster. On the other hand, outliers do not experience the attractive strong force as their average distance to other nuclei or nucleons is large. Therefore, their final potential energy is always positive. This allows for a simple identification of both clusters and outliers based on the $\bar{E}^{pot}$ histogram for all particles. As such, *Nuclear Potential Clustering* might also be used as a tool to detect and remove outliers from multidimensional datasets.

It was demonstrated that the algorithm works very efficient even on hard cluster problems such as a horseshoe surrounded by blops (Fig. 1). However, we have observed a sensitivity of our algorithm to changes in $R$. A small value of $R$ resulted in the splitting of larger groups whereas larger clusters were fused if $R$ was too large. The splitting of clusters exclusively happens at regions where the point density decreases due to statistical fluctuations. It is therefore an finite sampling effect which does not occur in larger groups with approximate constant feature space density. However, it might even be be advantageous to differentiate and identify such "touching" clusters in some applications. A similar problem occurs for points located at the border of larger clusters where the density decreases (see e.g. Fig.

ISBN: 978-988-19251-6-9
ISSN: 2078-0958 (Print); ISSN: 2078-0966 (Online)

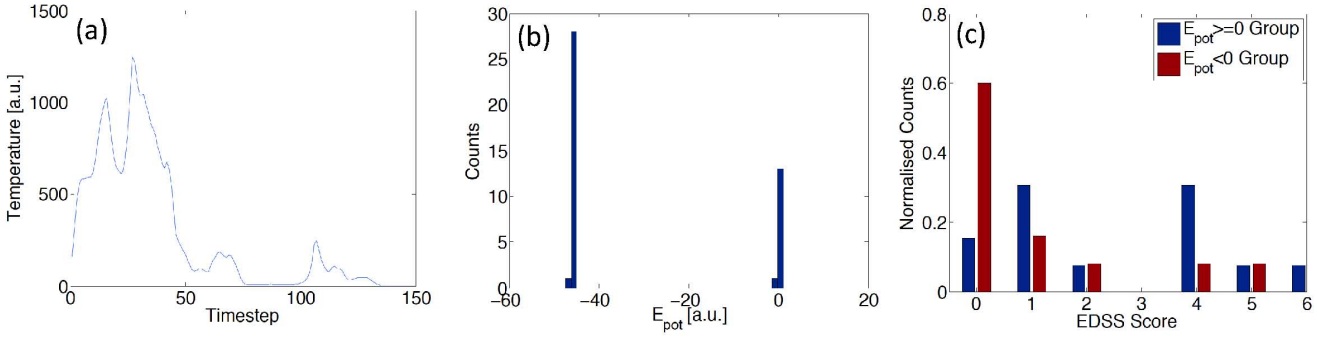


Fig. 2. Results from the unsupervised clustering of MS data. (a) Temperature as a function of time. (b) Final distribution of the potential energy for all points. The *Nuclear Potential Clustering* approach has identified one cluster with $\bar{E}^{pot} < 0$ and one outlier group. (c) Distribution of the EDSS score for the two groups identified. The outlier group has a significantly higher average EDSS score.

1(c)). Both cases might be handled by increasing the nuclear force range, $R$, in Eq. 1 during later stages of the algorithm. We do not expect that this poses significant problems in that distinct clusters are subsequently fused. As can be seen from Fig. 1, clusters are significantly shrunken to highly dense regions in feature space at later times. Therefore, a reasonable increase of $R$ should not result in a fusion of otherwise distinct clusters. The optimisation of the best choice for $R(t)$ is currently investigated in our lab.

Even though *Nuclear Potential Clustering* has proven a good performance on correlated multidimensional test datasets, several further improvements are possible. Most importantly, the final identification of clusters might be enhanced by adding additional features such as the cluster shape or position in feature space. Currently, the average potential energy of each point is used as single criterion to identify the number of clusters and to define the membership of each point to a cluster. This is because the average potential energy of a nucleon is given by the attractive potential of the $N-1$ other nucleons of the same nuclei. Therefore, all points in a common cluster experience approximately the same average $E^{pot}$. However, if two groups with the same number of members are present, the current criterion does not allow for a differentiation of the corresponding clusters. Therefore, additional measures such as the centre of mass or shape parameters have to be included to better differentiate distinct clusters which contain the same number of points.

### B. Quantitative MRI data

As discussed above, the method presented in the current work allows for a simulatanous identification of clusters and outliers. Applying the *Nuclear Potential Clustering* approach to image features derived from quantitative MRI maps revealed an interesting relationship. We have observed that younger patients with low grade disease without significant neurological symptoms form a homogeneous group (cluster). In contrast, older patients with higher grade were identified as outliers, i.e. they did not show a consistent behaviour with respect to the image features defined. This can be interpreted as a diffuse evolution of different disease courses of individual patients which start from a common region of feature space. It might be interesting for future studies to follow the time dependence of the path for an indidual patient in feature space in order to investigate and better characterise the underlying dynamic behaviour.

It is important to notice that this observation implies by no means that the dispersion of points is only due to differences in the individual disease courses. It might have been influenced by other factors, i.e. the different ages or treatment histories of the individual subjects. However, this article focusses on the feasibility of *Nuclear Potential Clustering* to detect meaningfull structures in MR image data. Therefore, a further clinical investigation and interpretation is outside the scope of this study.

The image features used for the classification of MS patients were all based on quantitative MRI acquisitions. Therefore, any feature calculated from a quantitative map is quantitative itself. Even though such parameters are highly correlated, their quantitative nature significantly simplifies the study of chronic diseases such as multiple sclerosis. This is because all parameters are solely influenced by physical and/or physiological changes within an image voxel. They do not depend on environmental factors such as scanner manufacturer, software, magnetic field strength or room temperature, which typically change between scans performed at different timepoints or different institutions. However, MS patients have to be scanned regulary resulting in up to 100 MR scans for an individual subject, performed over the period of several decades. Therefore, it is extremely important to define quantitative biomarkers which are independent of the changing environmental conditions. This might be one of the reasons why quantitative MR methods are extensively investigated in the MS-related literature [3], [7]. However, the emergence of new acquistion schemes, which allow for the simultaneous measurement of quantitative parameters within short measurement times [22]–[24], require the use of proper tools for the analysis of the corresponding multidimensional distributions. It was therefore the ultimate goal of the current work to present a new approach for the extraction of quantitative image based biomarkers. Such methods should provide a basis for future research efforts on markers for the objective assessment and therapy evaluation of multiple sclerosis.

## ACKNOWLEDGMENT

The author would like to thank Dr. Jochen Schenk for his kind support in providing access to a 3T MR scanner.

Dr. Andreas Böer is greatly acknowledged for his support in patient recruitment.

## REFERENCES

[1] E. Miller, "Multiple sclerosis," *Adv. Exp. Med. Biol.*, vol. 724, pp. 222–238, 2012.

[2] C. H. Polman, S. C. Reingold, G. Edan, M. Filippi, H. P. Hartung, L. Kappos, F. D. Lublin, L. M. Metz, H. F. McFarland, P. W. O'Connor, M. Sandberg-Wollheim, A. J. Thompson, B. G. Weinshenker, and J. S. Wolinsky, "Diagnostic criteria for multiple sclerosis: 2005 revisions to the "McDonald Criteria"," *Ann. Neurol.*, vol. 58, no. 6, pp. 840–846, Dec 2005.

[3] R. Bakshi, A. J. Thompson, M. A. Rocca, D. Pelletier, V. Dousset, F. Barkhof, M. Inglese, C. R. Guttmann, M. A. Horsfield, and M. Filippi, "MRI in multiple sclerosis: current status and future prospects," *Lancet Neurol*, vol. 7, no. 7, pp. 615–625, Jul 2008.

[4] A. Ceccarelli, R. Bakshi, and M. Neema, "MRI in multiple sclerosis: a review of the current literature," *Curr Opin Neurol*, Jun 2012.

[5] A. L. Liang, I. M. Vavasour, B. Madler, A. L. Traboulsee, D. J. Lang, D. K. Li, A. L. Mackay, and C. Laule, "Short-term stability of T (1) and T (2) relaxation measures in multiple sclerosis normal appearing white matter," *J. Neurol.*, vol. 259, no. 6, pp. 1151–1158, Jun 2012.

[6] H. Vrenken, A. Seewann, D. L. Knol, C. H. Polman, F. Barkhof, and J. J. Geurts, "Diffusely abnormal white matter in progressive multiple sclerosis: in vivo quantitative MR imaging characterization and comparison between disease types," *AJNR Am J Neuroradiol*, vol. 31, no. 3, pp. 541–548, Mar 2010.

[7] A. L. MacKay, I. M. Vavasour, A. Rauscher, S. H. Kolind, B. Madler, G. R. Moore, A. L. Traboulsee, D. K. Li, and C. Laule, "MR relaxation in multiple sclerosis," *Neuroimaging Clin. N. Am.*, vol. 19, no. 1, pp. 1–26, Feb 2009.

[8] F. Manfredonia, O. Ciccarelli, Z. Khaleeli, D. J. Tozer, J. Sastre-Garriga, D. H. Miller, and A. J. Thompson, "Normal-appearing brain t1 relaxation time predicts disability in early primary progressive multiple sclerosis," *Arch. Neurol.*, vol. 64, no. 3, pp. 411–415, Mar 2007.

[9] K. Schmierer, C. A. Wheeler-Kingshott, P. A. Boulby, F. Scaravilli, D. R. Altmann, G. J. Barker, P. S. Tofts, and D. H. Miller, "Diffusion tensor imaging of post mortem multiple sclerosis brain," *Neuroimage*, vol. 35, no. 2, pp. 467–477, Apr 2007.

[10] K. Schmierer, D. J. Tozer, F. Scaravilli, D. R. Altmann, G. J. Barker, P. S. Tofts, and D. H. Miller, "Quantitative magnetization transfer imaging in postmortem multiple sclerosis brain," *J Magn Reson Imaging*, vol. 26, no. 1, pp. 41–51, Jul 2007.

[11] H. Vrenken, S. A. Rombouts, P. J. Pouwels, and F. Barkhof, "Voxel-based analysis of quantitative T1 maps demonstrates that multiple sclerosis acts throughout the normal-appearing white matter," *AJNR Am J Neuroradiol*, vol. 27, no. 4, pp. 868–874, Apr 2006.

[12] D. Tozer, A. Ramani, G. J. Barker, G. R. Davies, D. H. Miller, and P. S. Tofts, "Quantitative magnetization transfer mapping of bound protons in multiple sclerosis," *Magn Reson Med*, vol. 50, no. 1, pp. 83–91, Jul 2003.

[13] C. Laule, I. M. Vavasour, G. R. Moore, J. Oger, D. K. Li, D. W. Paty, and A. L. MacKay, "Water content and myelin water fraction in multiple sclerosis. A T2 relaxation study," *J. Neurol.*, vol. 251, no. 3, pp. 284–293, Mar 2004.

[14] T. D. Nguyen, C. Wisnieff, M. A. Cooper, D. Kumar, A. Raj, P. Spincemaille, Y. Wang, T. Vartanian, and S. A. Gauthier, "T2 prep three-dimensional spiral imaging with efficient whole brain coverage for myelin water quantification at 1.5 tesla," *Magn Reson Med*, vol. 67, no. 3, pp. 614–621, Mar 2012.

[15] C. Lenz, M. Klarhofer, and K. Scheffler, "Feasibility of in vivo myelin water imaging using 3D multigradient-echo pulse sequences," *Magn Reson Med*, Dec 2011.

[16] D. Hwang, H. Chung, Y. Nam, Y. P. Du, and U. Jang, "Robust mapping of the myelin water fraction in the presence of noise: synergic combination of anisotropic diffusion filter and spatially regularized nonnegative least squares algorithm," *J Magn Reson Imaging*, vol. 34, no. 1, pp. 189–195, Jul 2011.

[17] D. Hwang, D. H. Kim, and Y. P. Du, "In vivo multi-slice mapping of myelin water content using T2* decay," *Neuroimage*, vol. 52, no. 1, pp. 198–204, Aug 2010.

[18] S. C. Deoni, B. K. Rutt, T. Arun, C. Pierpaoli, and D. K. Jones, "Gleaning multicomponent T1 and T2 information from steady-state imaging data," *Magn Reson Med*, vol. 60, no. 6, pp. 1372–1387, Dec 2008.

[19] Y. P. Du, R. Chu, D. Hwang, M. S. Brown, B. K. Kleinschmidt-DeMasters, D. Singel, and J. H. Simon, "Fast multislice mapping of the myelin water fraction using multicompartment analysis of T2* decay at 3T: a preliminary postmortem study," *Magn Reson Med*, vol. 58, no. 5, pp. 865–870, Nov 2007.

[20] J. Oh, E. T. Han, M. C. Lee, S. J. Nelson, and D. Pelletier, "Multislice brain myelin water fractions at 3T in multiple sclerosis," *J Neuroimaging*, vol. 17, no. 2, pp. 156–163, Apr 2007.

[21] T. Andrews, J. L. Lancaster, S. J. Dodd, C. Contreras-Sesvold, and P. T. Fox, "Testing the three-pool white matter model adapted for use with T2 relaxometry," *Magn Reson Med*, vol. 54, no. 2, pp. 449–454, Aug 2005.

[22] H. Neeb, V. Ermer, T. Stocker, and N. J. Shah, "Fast quantitative mapping of absolute water content with full brain coverage," *Neuroimage*, vol. 42, no. 3, pp. 1094–1109, Sep 2008.

[23] V. Arhelger, F. Kasten, D. Gliedstein, M.-S. Lafontaine, V. Tonkova, D. Holz, A. Böer, J. Schenk, and H. Neeb, "Rapid simultaneous mapping of total and myelin water content, $t1$ and $t_2^*$ in multiple sclerosis," 08 2010. [Online]. Available: http://arxiv.org/abs/1008.5038

[24] V. Tonkova, V. Arhelger, J. Schenk, and H. Neeb, "Rapid myelin water content mapping on clinical MR systems," *Z Med Phys*, vol. 22, no. 2, pp. 133–142, Jun 2012.

[25] R. O. Duda, P. E. Hart, and D. Stork, *Pattern Classification*. John Wiley And Sons, 2000.

[26] W. Heisenberg, *Nuclear Physics*. Citadel Press, Jan 1953.

[27] R. P. Feynman, *Quantum Electrodynamics*. Perseus, March 1998.

[28] S. M. Smith, M. Jenkinson, M. W. Woolrich, C. F. Beckmann, T. E. Behrens, H. Johansen-Berg, P. R. Bannister, M. De Luca, I. Drobnjak, D. E. Flitney, R. K. Niazy, J. Saunders, J. Vickers, Y. Zhang, N. De Stefano, J. M. Brady, and P. M. Matthews, "Advances in functional and structural MR image analysis and implementation as FSL," *Neuroimage*, vol. 23 Suppl 1, pp. S208–219, 2004.

[29] H. Neeb, K. Zilles, and N. J. Shah, "Fully-automated detection of cerebral water content changes: study of age- and gender-related H2O patterns with quantitative MRI," *Neuroimage*, vol. 29, no. 3, pp. 910–922, Feb 2006.

[30] R. D. Woods and D. S. Saxon, "Diffuse surface optical model for nucleon-nuclei scattering," *Phys. Rev.*, vol. 95, pp. 577–578, 1954.